Arabian Journal of Chemistry (2013) 6, 319–326

King Saud University

Arabian Journal of Chemistry

www.ksu.edu.sa
www.sciencedirect.com

ORIGINAL ARTICLE

Synthesis and performance characterization of PS-PPEES nanoporous membranes with nonwoven porous support

Chitrakara Hegde [a], Arun M. Isloor [b,*], Mahesh Padaki [c], Hoong-Kun Fun [d]

[a] *Department of Chemistry Alliance College of Engineering and Design Alliance University Chikkahagade Cross Chandapur-Anekal Main Road Bangalore-562106*
[b] *Membrane Technology Division, Department of Chemistry, National Institute of Technology-Karnataka, Surathkal, Mangalore 575 025, India*
[c] *Centre for Nano and Materìaì Sciences, Jain University, Jakasand ra, Bangalore-5621 12*
[d] *Department of Pharmaceutical Chemistry College of Pharmacy, King Saud University P.O. Box. 2457 - Riyadh 11451, Kingdom of Saudi Arabia*

Received 18 January 2011; accepted 23 May 2011
Available online 30 June 2011

KEYWORDS

PS-PPEES;
Nonwoven support;
Flux;
Salt rejection;
Proton conductivity

Abstract The present work describes about the synthesis and characterization of Polysulfone blend nanoporous membrane with nonwoven support. This Nonwoven support provides mechanical strength to membrane while filtration process and minimizes membrane fouling. Hence it helps in better membrane performance in terms of salt rejection, improved flux, thermal stability and fairly increases in proton conductivity. In this work we have used K.C.270 nonwoven material consisting of fine polyester fibers and has a thickness of below 110 μm.

1. Introduction

In the recent past, membrane processes gradually have found their way into industrial applications and serve as viable alternatives for more traditional processes like distillation, evaporation or extraction. Different membranes are categorized and they are used for different purpose of separation process, depending on their physical and chemical properties (Lhassani et al., 2001). Among membranes, Nanofiltration (NF) membrane is characterized by its surface charge and Nano pore size (Szymczyk et al., 2003). NF membrane shows high efficiency with a reasonable water flux at relatively low pressures, therefore Nanofiltration (NF) membranes are used in a wide range of drinking water, wastewater, (Al-Sofi, 2001) and industrial applications (Van der Bruggen and Vandecasteele, 2003). Nanofiltration (NF) membranes can retain multivalent ions (e.g., calcium, magnesium, aluminum, sulfates) (Bowen et al.,

* Corresponding authors. Address: Membrane Technology Division, Department of Chemistry, National Institute of Technology, Surathkal, Mangalore 575 025, India. Tel.: +91 824 2474000x3206; fax: +91 824 2474033.
E-mail address: isloor@yahoo.com (A.M. Isloor).

1878-5352

Peer review under responsibility of King Saud University.
doi:10.1016/j.arabjc.2011.05.014

Production and hosting by Elsevier

1997) and non-ionized organic compounds with a molar mass exceeding about 300 g/mol. Hence it shows potential applications such as selective demineralization (for water softening) (Schaep et al., 1998) and concentration of organic compounds with low molar mass. As a consequence, scientists and industrialists nowadays feel more confident about what can be expected from a NF membrane, and more and more applications proved to be successful including water treatment, wastewater and desalination of dyestuffs, acid and caustic recovery and color removal (Zhijuan et al., 2006). In this study polysulfone based novel NF membranes were synthesized and their characterizations were made based on T_g, proton conductivity and flux rejection study. Above mentioned performance study gave a number of conclusions which are very helpful in this further research.

It is a well known fact that membrane filtration technology was greatly limited by membrane fouling. Membrane fouling phenomenon increases operation and maintenance costs by deteriorating membrane performances (flux decline vs. time, zeta potential changing during time, etc.) and eventually shortening membrane life (Ahmed and Robert, 2007). Hence it is sensible to use nonwoven porous support which generally has the superior dirt holding capacity and does not have a much wider pore size distribution. Such quality along with reinforcement of mechanical strength to the membranes gives better performance with decreased fouling (Violleau et al., 2005).

2. Experimental

2.1. Materials and instruments

Polysulfone having molecular weight of 35,000 PS, poly(1,4-phenylene ether ether-sulfone), PPEES were obtained from Sigma Aldrich in the form of semitransparent beads. Reagent grade N-methyl pyrrolidone, NMP was obtained from Merck-India and was used without any further purification. Non woven support, was from K.C.270 Cranemat KC & SC made up of polypropylene. All analytical grade chemical reagents used in the experiment were purchased from Merck India Ltd. Glucose, sucrose and polyethylene glycols (PEGs 600, 800, 1000 Da) for the MWCO test were measured using CL 157 Colorimeter. IR spectra were recorded using Nicolet Avatar 5700 FTIR (Thermo Corporation) spectrometer. Impedance study was done using ACM Instruments, England. SEM images of the cross section of the newly prepared membranes were recorded on Jeol JSM-84. DSC study was carried out on a Shimadzu DSC 60 instrument, Japan. The permeation experiments were performed by a self fabricated salinity checking apparatus with membrane disk which has an effective area of 6.5 cm^2. The deionized water used for preparation of the salt solutions was obtained through demineralization using ion exchange followed by reverse osmosis. Surface roughness was determined using Atomic Force Microscopy (Nanosurf, EasyScan2).

2.2. Membrane synthesis

Solutions containing different wt.% of PS and PPEES (Table 1) in 4.5 ml of 1-methyl-2-pyrrolidone (NMP) were prepared by mild stirring for one day at constant temperature of 75 °C. So obtained viscous solution was casted over non woven support (K.C.270) using K-Control coater. Casted membrane was again heat-treated for 45 s at 220 °C, then washed thoroughly with deionized water and immersed in de-ionized water for 24 h (Chitrakara et al., 2011).

Table 1 Solutions containing different wt.% of PS and PPEES.

Membrane code	Wt.% composition (PS)	Wt.% composition (PPEES)
M1	90	10
M2	80	20
M3	70	30
M4	60	40

Table 2 Water uptake results of newly synthesized NF membranes with nonwoven support.

Membrane code	Water up-take
M1	45%
M2	57%
M3	68%
M4	72%

2.3. Water up take

The swelling characteristics were determined by water uptake measurements. The membrane samples were first immersed in deionized water until there was no weight difference in the membrane. Further wet membrane then blotted to dry to remove surface droplets was quickly weighed. The wet membranes were vacuum dried at 80–100 °C and weighted again. The water uptake of the membranes was calculated by weight gain of absorbed water with reference to the dry membrane and reported as weight percent water absorption. The water uptake can be calculated as follows (Chitrakar et al., 2009).

$$\text{Water uptake} = m_{wet} - m_{dry}/m_{dry}$$

where m_{wet} is the weight of wet membrane and m_{dry} is the weight of dry membrane. The result of the same has been presented in Table 2. These observed water uptakes are much more than our earlier work (Chitrakar et al., 2009).

2.4. Permeation experiment

Salts with different valence distribution are used for NF membrane experiments to investigate membrane properties. The permeability of pure water through this NF membrane was also measured. Flux, F (l/m^2 h), was calculated as Eq. (1):

$$F = W/At \quad (1)$$

where W (l) is the total volume of the water or solution permeated during the experiment, A (m^2) is the membrane area, and t (h) is the operation time. Rejection, R, is calculated as Eq. (2):

$$R = (1 - \text{concentrate permeates/concentrate feed}) \quad (2)$$

Schematic diagram of lab scale filtration set up is shown in Fig. 1. The feed was taken from the feed tank and was pumped into the module. The pressure difference between the feed inlet and the outlet during operation was adjusted from 1 to 14 Bar.

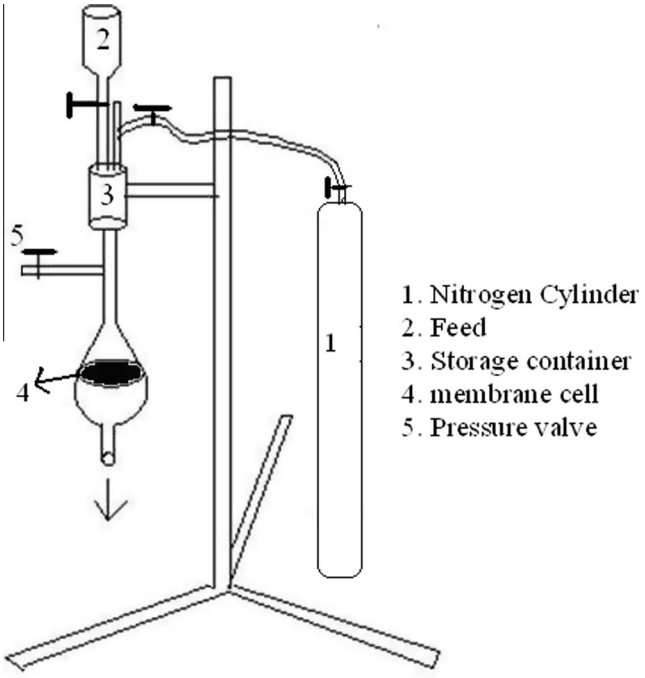

Figure 1 Schematic representation of the self made salinity checking unit.

The rate of the permeate stream was measured by a rotameter and a gauged cylinder where as rejection (%) was studied by conductivity measurements (Toshinori et al., 2010).

2.5. Membrane hydraulic resistance (R_h)

To determine the Membrane hydraulic resistance (R_h), the pure water flux of the membrane was measured at different transmembrane pressure (ΔP). The variation of pure water flux was plotted as a function of transmembrane pressure for all the prepared membranes. Membrane hydraulic resistance (R_m) was determined from the inverse of slopes, using following equation (Abdoul et al., 2007).

$$R_h = \Delta P/F, \text{ where } F = \text{pure water flux } (l/m^2h) \quad (3)$$

2.6. Molecular weight cut-off (MWCO)

Molecular weight cut-off or MWCO refers to the lowest molecular weight solute (in Daltons) in which 90% of the solute is retained by the membrane or the molecular weight of the molecule (e.g., globular protein) that is 90% retained by the membrane. To determine the MWCO for the resultant membrane, solutes with molecular weight range of 180–1000 Da were chosen, namely glucose, sucrose and polyethylene glycols (PEGs 600, 800, 1000 Da) at a concentration of 1000 mg/L. The rejection was obtained according to Eq. (2) (Ruihua et al., 2009).

2.7. Structural characterization

Surface analysis can be done with different tools, each one with its own specificity with regard to the conditions of use and to the information it provides. In our study, we used scanning electron microscope (SEM) and an atomic force microscope (AFM). The membrane was cryogenically fractured in liquid nitrogen and then sputtered with gold. SEM provides information on surface porosity and layer thickness. To prepare samples for AFM, the membranes were dried in vacuum at room temperature. The membranes were taken out of water and air-dried and they were ready for AFM observation. AFM Imaging was performed in tapping mode with resonant frequency of 200–400 kHz, nominal tip radius of 5–10 nm. Atomic force microscopy (AFM) provides surface RMS roughness (Chitrakar et al., 2009, 2011).

2.8. DSC analysis

Differential-scanning calorimetry is a thermodynamic technique widely used for studying thermal characteristics of the membrane. The ability to monitor phase transitions in polymeric membrane has not only provided data on thermodynamic stability for these important molecules, but also made it possible to examine the details of unfolding processes and to analyze the characteristics of intermediate states involved in the melting of membrane polymers. It is well known that PS has a high melting point and hydrophobic. A DSC-60 Shimadzu calorimeter was used to analyze the thermal behavior of differently processed membranes, with the heating rate of 15 °C /min up to 300 °C. DSC curve of the resultant membranes were studied with increase in temperature at the rate of 10 °C/min. Each sample was subjected to several heating/cooling cycles to obtain reproducible T_g values. The initial onset of the change midpoint of slope in the DSC curve is taken to be the T_g (Helen et al., 2007; Sturtevant, 1996).

3. Results and discussion

3.1. Pure water permeability

At different pressure (bar), flux for pure water is shown in Fig. 2. The plot depicts a linear relationship between the pure water flux and transmembrane pressure. It is seen that there is a slow and steady increase of pure water flux with respect to decrease in PS wt.%. This is due to the fact that PPEES leads predominantly to swelling rather than leaching out from the membrane-forming system. Consequently, the flow path in

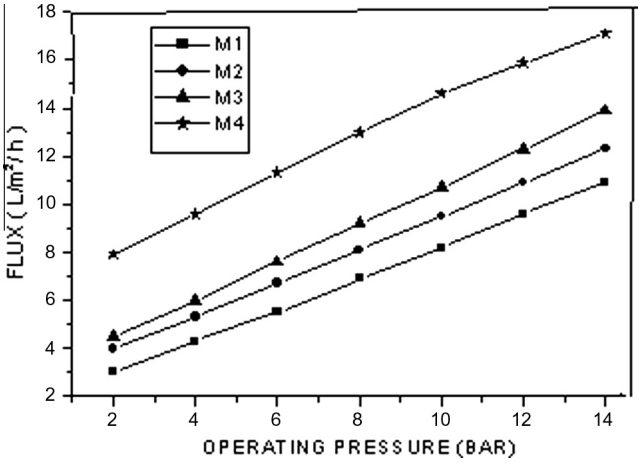

Figure 2 Pure water flux at different pressure (bar).

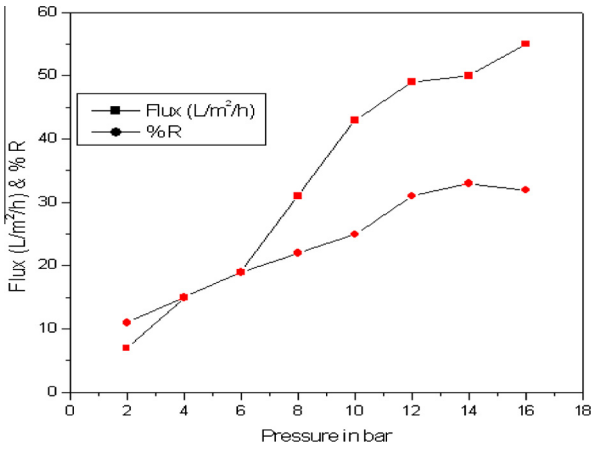

Figure 3 Performance of membrane M4 with operating pressure.

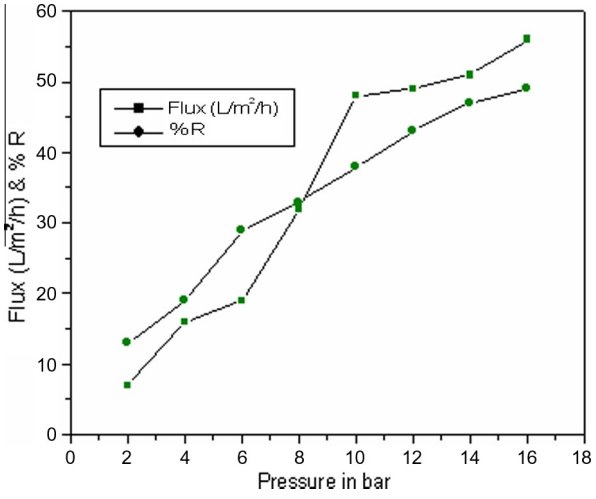

Figure 4 Performance of membrane M3 with operating pressure.

the membrane was reduced and hence the increase in the flux was not steep. Flux values of M1 and M2 further reinforces above explanation (Ruihua et al., 2009).

3.2. Membrane hydraulic resistance (R_m)

Membrane hydraulic resistance was calculated from the inverse of slopes of the corresponding water flux versus pressure lines and is shown in Table 3. It is evident from these values that as the concentration of PS increases in the blend system, the R_m decreases. This can be explained by the fact that PS is relatively more hydrophobic in nature whereas increase in PPEES leads to the formation of pores, which in turn increases the flux thereby decrease in membrane resistance (Sivakumar et al., 2000). The values of the same have been represented in Table 3.

3.3. Effect of operating pressure on membrane performance

To illustrate the effect of operating pressure on newly synthesized membrane, the feed concentration (NaCl) was fixed at

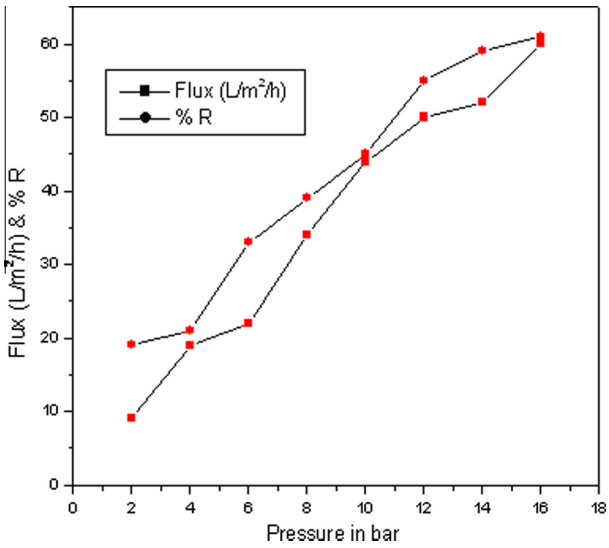

Figure 5 Performance of membrane M2 with operating pressure.

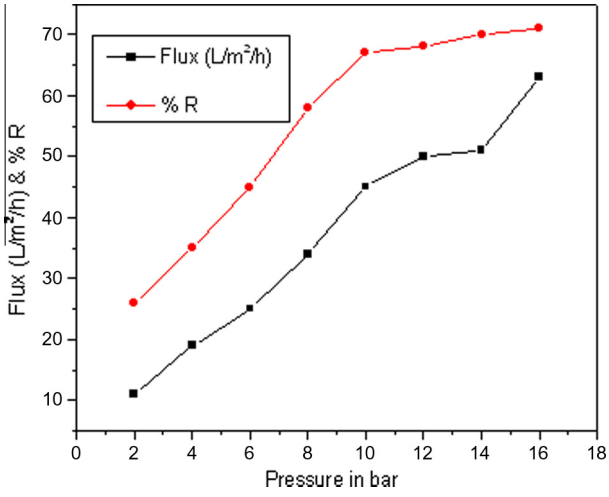

Figure 6 Performance of membrane M1 with operating pressure.

1000 mg/L. Water flux across the membrane increases in direct relationship with increase in feed water pressure but the rejection of salts by the NF membrane is more complicated as it is depends on both molecular size and Donnan exclusion effects (Szymczyk et al., 2003), it is well understood that solute (NaCl) is hydrophilic in nature where as membrane as a whole is hydrophobic. This hydrophobic interaction makes minimum passage for salt, thus as shown in Figs. 3–6 increased feed water pressure increases salt rejection but, to a lower extent than water flux. Because NF membranes are imperfect barriers to dissolved salts in feed water, there is always some salt passage through the membrane. As feed water pressure is increased, this salt passage is increasingly overcome as water is pushed through the membrane at a faster rate than salt can be transported. However, there is an upper limit to the amount of salt that can be excluded via increasing feed water pressure. As the plateau in the salt rejection curve (Figs. 3–6) indicates,

above a certain pressure level, salt rejection no longer increases and some salt flow remains coupled with water flowing through the membrane.

3.4. Effect of feed concentration on membrane performance

To describe the effect of feed concentration on membranes, $MgCl_2$ and NaCl solutions with different concentration were used. The results are shown in Tables 4 and 5 respectively. Both the rejection and flux decrease with an increase in feed concentration, especially the NaCl solution. As the feed concentration increases, the repulsion effect of the charged membrane on the ions in feed decreases, leading to a lower rejection; meanwhile the double electrical layer near to membrane surface became thicker, thus the flux decreased (Petersen, 1993).

Table 3 Hydraulic resistance of the different membranes.

Membrane code	Hydraulic membrane resistance (R_m), m^2 h/L
M1	1.45
M2	1.36
M3	1.27
M4	1.19

Table 4 Effect of feed concentration on membrane performance at operating conditions 12 Bar.

Membrane code	$MgCl_2$ feed concentration, mg/L	Flux, L/m^2/h	%R
M1	1000	46	68
	2000	37	51
	3000	30	44
M2	1000	50	65
	2000	35	58
	3000	29	51
M3	1000	42	62
	2000	39	59
	3000	28	48
M4	1000	40	60
	2000	37	52
	3000	29	47

Table 5 Effect of feed concentration on membrane performance at operating conditions 12 Bar.

Membrane code	NaCl feed concentration, mg/L	Flux, L/m^2/h	%R
M1	1000	47	67
	2000	33	57
	3000	29	41
M2	1000	46	60.2
	2000	32	56
	3000	27	35
M3	1000	38	57
	2000	37	54
	3000	25	46
M4	1000	35	55
	2000	40	50
	3000	28	43

Table 6 Effect of the salt solution on membrane performance at operating conditions 12 Bar.

Salt conc., 2000 mg/L	Flux, L/m^2/h	%R
$MgCl_2$	35	55
$MgSO_4$	43	43
Na_2SO_4	39	40
K_2SO_4	42	33
KCl	39	38.5
$CaCl_2$	43	60
NaCl	31	45

3.5. Effect of the salt solution on membrane performance

The average rejection and flux of different synthesized membranes (M1, M2, M3 and M4) for salt solutions are listed in Table 6. The rejection order is $CaCl_2 > MgCl_2 > MgSO_4 > NaCl > KCl > Na_2SO_4 > K_2SO_4$. For $CaCl_2 > MgCl_2 > NaCl > KCl$ and $MgSO_4 > Na_2SO_4 > K_2SO_4$, corresponding to the increasing order of the cation charge densities, because the active layer has quaternary ammonium groups contribution and has a stronger repulsion to Mg^{2+} and Ca^{2+} than Na^+ and K^+, Mg^{2+} and Ca^{2+} are rejected easily. However, for $MgSO_4 > NaCl$, it may be speculated that the repulsion force on cation is much stronger than the attraction one on anion.

3.6. MWCO of membrane

The curve for the rejection for the model organic solutions against molecular weight is shown in Fig. 7. The MWCO was the molecular weight of organic substance with a rejection of 90%. The MWCO of the all resultant membrane lies approximately between 900 Da to 910 Da.

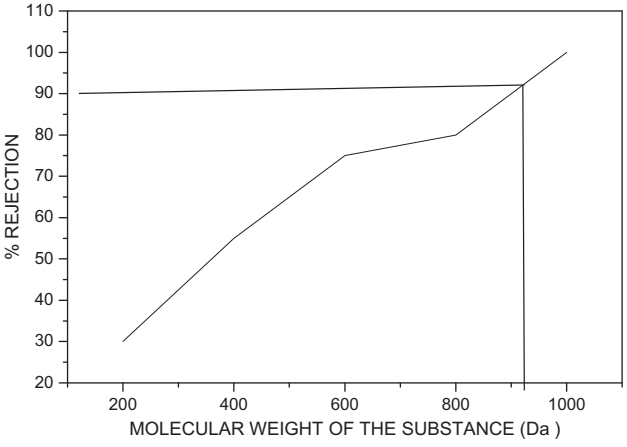

Figure 7 MWCO curve for newly synthesized NF membrane.

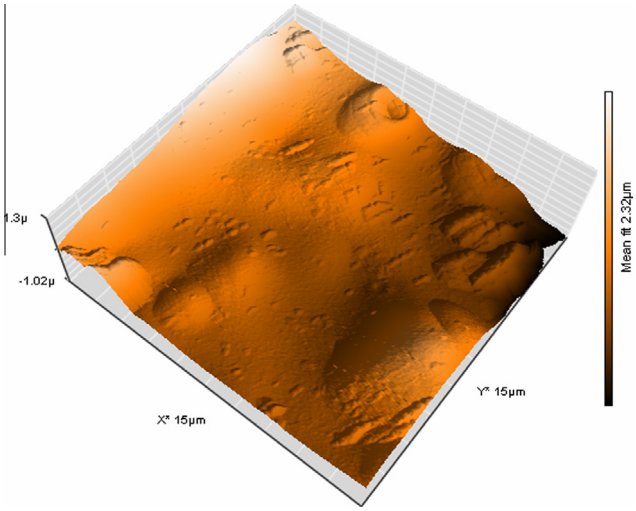

Figure 8 AFM surface roughness image of membrane M1.

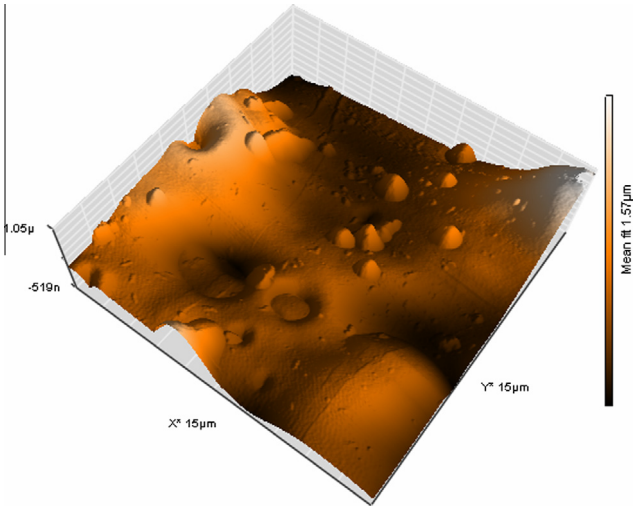

Figure 9 AFM surface roughness image of membrane M4.

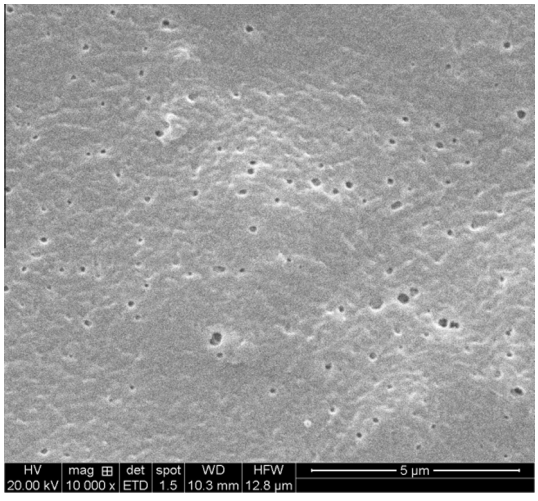

Figure 10 SEM surface image of the membrane M4.

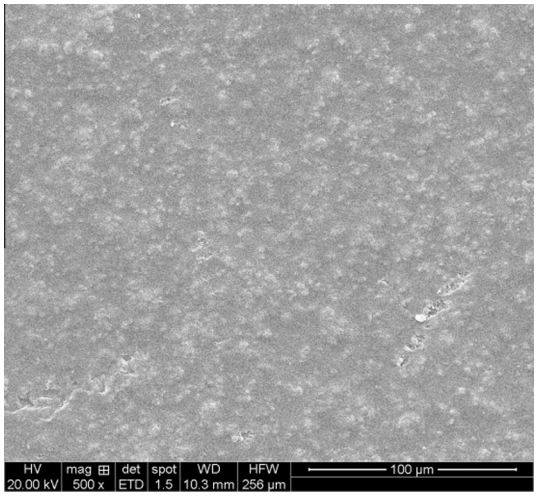

Figure 11 SEM surface image of the membrane M1.

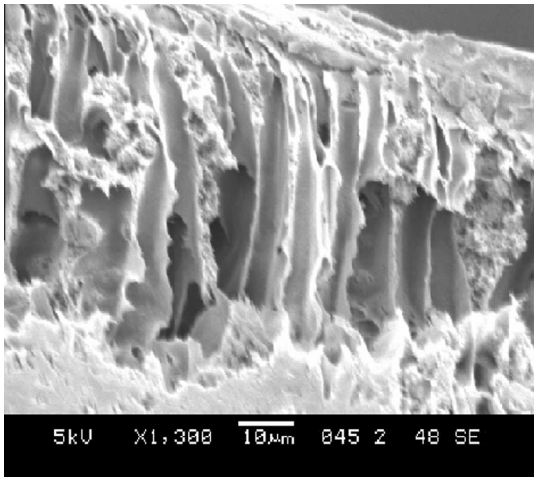

Figure 12 SEM cross section image of the membrane M4.

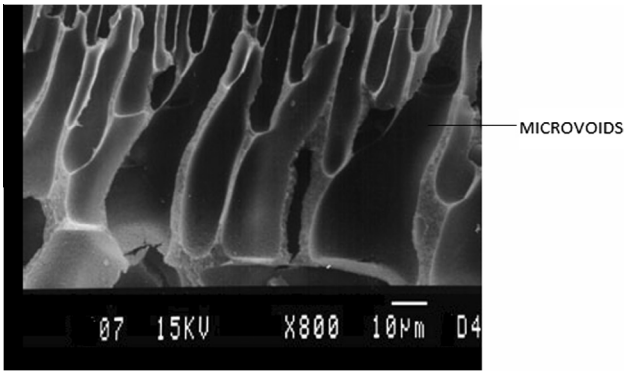

Figure 13 SEM cross section image of the membrane M1.

3.7. Morphology of membrane

Tapping mode AFM images give information related to surface features of the membranes. Figs. 8 and 9 show the surface

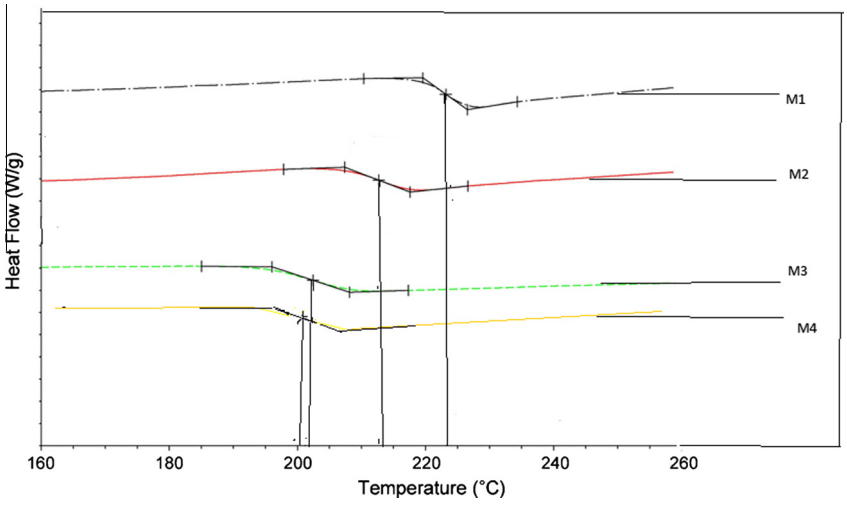

Figure 14 DSC curve of the membranes.

Table 7 T_g values of the membranes.

Membrane code	T_g (°C)
M1	223
M2	213
M3	203
M4	200

profile of membrane M1 and membrane M4 respectively. The membrane containing 90 wt.% of PS shows almost smooth and less intense crater and valley (Fig. 8) with reduced surface roughness rather than more surface roughness as like in M4 (Fig 9). This reduction in roughness of membrane clearly affirmed that PPEES incorporated well with PS matrix. Such a membrane matrix may give smooth electrical connectivity leading to better ionic conductivity. This explanation matches with our proton conductivity data (Pramod et al., 2010). Figs. 10 and 11 show the surface SEM pictures of membranes M4 and M1 respectively. The cross-section image of the composite membrane in Figs. 12 and 13 clearly shows that there is a thin selective layer on a finger-like 'micro voids' support layer suggesting the composite structure of this membrane. Meanwhile, the surface picture (Figs. 10 and 11) gives an overall view of pore size and pore distribution from SEM image, it is certain that the spongy layer provides the sustained structure that could support high pressure. The porous finger-like layer allows transporting the permeated solvent (Blanco et al., 2006).

3.8. DSC analysis

Fig. 14 shows the thermograms of DSC measurement of the membranes. The T_g values of the M1, M2, M3, M4 membranes are 223, 213, 203, 200 °C, respectively. The relationship between T_g and the composition of blended membranes depends upon percentage of poly sulfone, lower PS composite membrane shows T_g range from 200 °C to 203 °C whereas higher PS composition show T_g range from 213 °C to 223 °C. Table 8 shows the T_g values of the synthesized membranes. Results were summarized in Table 7.

4. Conclusion

The result shows newly synthesized NF membrane has better salt rejection performance capacity than our previous work on NF membrane without nonwoven porous support. Increased performance of membrane confirms that supporting material (K.C.270) helps in minimizing membrane fouling. Present membrane shows increased rejection percentage for divalent cation than monovalent cation. Noticeable increase in the water uptake was observed, which play vital role in proton hoping to exhibit proton conductivity. Interestingly it was observed that, increase in polysulfone concentration increases T_g value whereas increase in PPEES content increases number of pores.

Acknowledgments

The Authors extend their appreciation to The Deanship of Scientific Research at King Saud University for the funding the work through the research group project No. RGP-VPP-207.

References

Abdoul, R.J., Arthanreeswaran, G., Thanikaivelan, P., Mohan, D., Raajenthiren, M., 2007. Performance characterization of cellulose acetate and poly(vinylpyrrolidone)blend membranes. journal applied polymer science 04, 3042–3049.

Ahmed, Al-Amoudi, Robert, Lovitt, 2007. Fouling strategies and the cleaning system of NF membranes and factors affecting cleaning efficiency. J. Membrane Sci. 303(1–2), 4–28.nd NF membrane systems for drinking water production.

Al-Sofi, M., 2001. Seawater desalination - SWCC experience and vision. Desalination. 135 (1–3), 121–139.

Blanco, J.F., Sublet, J., Nguyen, Q.T., Schaetzel, P., 2006. Formation and morphology studies of different polysulfones-based membranes made by wet phase inversion process. Journal of membrane science 283, 27–37.

Bowen, W.R., Mohammad, A.W., Hilal, N., 1997. Characterisation of nanofiltration membranes for predictive purpose - use of salts, uncharged solutes, and atomic force microscopy. Journal of Membrane Science 126, 91–105.

Chitrakar, H., Mahesh, P., Arun, M.I., 2009. Synthesis, characterization and impedance study of some novel nanofiltration membranes. Iraqi J. Polym. 13 (2), 1–12.

Chitrakara, H., Arun, M.I., Mahesh, P., Pikul, W., Yu, L., 2011. Synthesis and desalination performance of Ar^{+}–N^{+} irradiated polysulfone based new NF membrane. Desalination 265 (1–3), 153–158.

Helen, M., Viswanathan, B., Srinivasa Murthy, S., 2007. Synthesis and characterization of composite membranes based on -zirconium phosphate and silicotungstic acid. Journal of Membrane Science 292, 98–105.

Lhassani, A., Rumeau, M., Benjelloun, D., Pontie, M., 2001. Selective demineralization of water by nanofiltration – application to the defluorination of brackish water. Water Res. 35 (13), 3260–3264.

Petersen, R.J., 1993. Composite reverse osmosis and nanofiltration membrane. Journal of Membrane Science 83, 81–150.

Pramod K. Singh, Bhattacharya, B., Nagarale, R.K., Kang-Wook Kim., Hee-Woo Rhee., 2010. Synthesis, characterization and application of biopolymer-ionic liquid composite membranes. Synthetic Metals 160,139–142.

Ruihua, H., Guohua, C., Mingkun, S., Congjie, G., 2009. Preparation and characterization of composite NF membrane from a graft copolymer of trimethylallyl ammonium chloride onto chitosan by toluene diisocyanate cross-linking. Desalination 239, 38–45.

Schaep, J., Van der Bruggen, B., Uytterhoeven, S., Croux, R., Vandecasteele, C., Wilms, D., Van Houtte, E., Vanlerberghe, F., 1998. Removal of hardness from groundwater by nanofiltration. Desalination 119, 295–302.

Sivakumar, M., Malaisamy, R., Sajitha, C.J., Mohan, D., Mohan, V., Rangarajan, R., 2000. Preparation and performance of cellulose acetate-polyurethane blend membranes and their applications II. Journal of Membrane Science 169, 215–228.

Sturtevant, J.M., 1996. Calorimetric studies of biopolymers. Protein Sci 5, 391–394.

Szymczyk, A., Labbez, C., Fievet, P., Vidonne, A., Foissy, A., Pagetti, J., 2003. Contribution of convection, diffusion and migration to electrolyte transport through nanofiltration membranes. Adv. Colloid Interface Sci 103, 77–94.

Toshinori, T., Kazuhisa, O., Masakoto, K., Tomohisa, Y., 2010. Permeation Characteristics of Electrolytes and Neutral Solutes through Titania Nanofiltration Membranes at High Temperatures. Langmuir 26 (13), 10897–10905.

Van der Bruggen, B., Vandecasteele, C., 2003. Removal of pollutants from surface water and groundwater by nanofiltration: overview of possible applications in the drinking water industry. Environ. Poll. 122, 435–445.

Violleau, D., Essis-Tome, H., Habaroub, H., Croué, J.P., Pontié, M., 2005. Fouling studies of a polyamide nanofiltration membrane by selected natural organic matter: an analytical approach. Desalination 173, 223–238.

Zhijuan, J., Yasan, H., Guojun, Z., 2006. Treatment of wastewater during the production of reactive dyestuff using a spiral nanofiltration membrane system. Desalination 201 (1–3), 255–266.